ResearchGate

See discussions, stats, and author profiles for this publication at: https://www.researchgate.net/publication/306086330

An oscillating wave energy converter with nonlinear snap-through Power-Take-Off systems in regular waves

Article *in* China Ocean Engineering · July 2016

DOI: 10.1007/s13344-016-0035-5

CITATIONS
0

READS
50

3 authors, including:

Xiantao Zhang
University of Western Australia
13 PUBLICATIONS **10** CITATIONS

SEE PROFILE

Some of the authors of this publication are also working on these related projects:

Green water for ship-type offshore structures View project

All in-text references underlined in blue are linked to publications on ResearchGate, letting you access and read them immediately.

Available from: Xiantao Zhang
Retrieved on: 20 October 2016

China Ocean Eng., Vol. 30, No. 4, pp. –
© 2016 Chinese Ocean Engineering Society and Springer-Verlag Berlin Heidelberg
DOI, ISSN 0890-5487

An Oscillating Wave Energy Converter with Nonlinear Snap-Through Power-Take-Off Systems in Regular Waves*

ZHANG Xian-tao (张显涛)[a], YANG Jian-min (杨建民)[a, 1] and XIAO Long-fei (肖龙飞)[a]

[a] *State Key Laboratory of Ocean Engineering*, *Shanghai Jiao Tong University*, *Shanghai 200240*, *China*

(Received 17 February 2014; received revised form 6 February 2015; accepted 18 April 2015)

ABSTRACT

Floating oscillating bodies constitute a large class of wave energy converters, especially for offshore deployment. Usually the Power-Take-Off (PTO) system is a directly linear electric generator or a hydraulic motor that drives an electric generator. The PTO system is simplified as a linear spring and a linear damper. However the conversion is less powerful with wave periods off resonance. Thus, a nonlinear snap-through mechanism with two symmetrically oblique springs and a linear damper is applied in the PTO system. The nonlinear snap-through mechanism is characteristics of negative stiffness and double-well potential. An important nonlinear parameter γ is defined as the ratio of half of the horizontal distance between the two springs to the original length of both springs. Time domain method is applied to the dynamics of wave energy converter in regular waves. And the state space model is used to replace the convolution terms in the time domain equation. The results show that the energy harvested by the nonlinear PTO system is larger than that by linear system for low frequency input. While the power captured by nonlinear converters is slightly smaller than that by linear converters for high frequency input. The wave amplitude, damping coefficient of PTO systems and the nonlinear parameter γ affect power capture performance of nonlinear converters. The oscillation of nonlinear wave energy converters may be local or periodically inter well for certain values of the incident wave frequency and the nonlinear parameter γ, which is different from linear converters characteristics of sinusoidal response in regular waves.

Key words: *wave energy*; *power-take-off*; *snap-through*; *time domain equation*; *state space*; *dynamic response*

1. Introduction

Floating oscillating-body devices constitute a large class of wave energy converters, especially for offshore deployment, the typical depth of which is between 40 and 100 m (Falcão, 2010). For such devices, the oscillating motion (rectilinear or angular) of a floating body or the relative motion between two moving bodies is converted into electricity by the Power-Take-Off (PTO) system (Zhang Y. Q. *et al.*, 2014). One typical PTO system is a linear electric generator directly driven by the motion of the oscillating body; another one is a hydraulic motor (or a high-head water turbine) that drives an electric generator (Vicente *et al*., 2013; Zhang D. H. *et al.*, 2014). Usually the PTO system is simplified as a linear spring and a linear damper along the direction of oscillation. Thus frequency domain models (Gomes *et al*., 2012) are widely used due to its simplicity and low computer requirement. Falnes (2002) studied a single degree-of-freedom oscillating body with linear PTO system using the frequency model and pointed out, for a sinusoidal regular wave input, that the maximum power is obtained at the state of

* This work was financially supported by the National Natural Science Foundation of China (Grant No. 51239007) and the Independent Research Project of State Key Laboratory of Ocean Engineering in Shanghai Jiao Tong University (Grant No. GKZD010023).
1 Corresponding author. E-mail: jmyang@sjtu.edu.cn

resonance, when the natural frequency of the converter corresponds to the exciting one, together with radiation damping equaling to the PTO conversion damping. However, frequency domain method cannot be applied to such cases as large displacement, nonlinear restoring or damping forces associated to PTO systems and so on (Alves, 2012). Thus, time-domain analysis, which was first applied to ships in wavy sea by Cummins (1962), is used to dynamic responses of floaters' oscillation with nonlinear characteristics.

The oscillating wave energy converter with linear PTO systems is characteristic of frequency-dependent response showing the phenomenon of resonance. However, the conversion is less powerful with wave periods off resonance, in particular the resonance bandwidth is narrow. As a result, it motivates us to make use of nonlinear oscillators in PTO system for enhanced energy-harvesting performance. Nonlinear oscillators were first studied in the realm of vibration energy harvesting instead of ocean wave energy utilization. The device with mechanical nonlinearity may perform better compared with standard linear devices. The use of a nonlinear mechanism consisting of a nonlinear hardening spring has been proposed by Burrow and Clare (2007) and Mann and Sims (2009), and they described the benefits of using a hardening spring instead of a linear spring in terms of bandwidth over which the device can perform well, based on the simulation and experimental results. Ramlan *et al*. (2010) studied two nonlinear oscillators, one is the snap-through mechanism, which is also called bistable oscillators, and the other is the nonlinear hardening spring together with a linear damper. The response of the nonlinear oscillator is periodic or chaotic under a sinusoidal periodic input. Also an analytical expression was derived to describe the bandwidth of the system with a hardening spring. Ma (2011) performed theoretical and numerical studies on the nonlinear oscillator excited by a linear impulsively loaded structure. Only the type of nonlinearity represented by a cubic structural stiffness coefficient was considered. His studies showed that a device designed with proper nonlinearity may harvest more energy than its linear counterpart if there is a significant frequency mismatch. Harne and Wang (2013) made a summary of the recent research on vibration energy harvesting via nonlinear snap-through systems.

The main objective of this paper is to study the nonlinear snap-through mechanism consisting of two symmetrically oblique springs and a linear damper in the PTO system of the oscillating-body wave energy converters in regular waves. Time domain equation is used to study the dynamic response of the oscillating wave energy converter with both linear and nonlinear snap-through PTO systems. And state-space model (Alves, 2012) is used to replace the convolution terms due to its inconvenience in analyzing the dynamic response of oscillating floaters. The response of displacement and velocity, as well as the harvesting energy is obtained numerically for both linear and nonlinear PTO system. Comparisons of power capture are made between the two converters. The effects of wave amplitude, the nonlinear parameter γ and damping coefficient of PTO systems on power capture are also analyzed. Finally, the characteristics of oscillation of wave energy converters with linear and nonlinear snap-through PTO mechanism are studied in detail.

2. Model of Nonlinear and Linear Converters

A hemisphere floating under the water surface is adopted as the geometry for the converter. And the

hemisphere is rigidly connected to the nonlinear snap-through PTO systems, consisting of a damper and two symmetrically oblique springs (Fig. 1). This is quite different from the general linear PTO systems, which is comprised of a linear damper and a linear spring (Fig. 2). The joint of the hemisphere is located at the floater's center, which allows the pitch oscillation and the rotational inertia to be neglected. Therefore, only the heave oscillation is considered for simplified cases. And due to the geometrical symmetry of the converter, one-directional waves are assumed. It should also be mentioned that neither the elasticity of the rigid connection unit nor the friction inside the PTO systems is considered. The draught of the hemispherical floater in still water equals its radius. Finally, the water depth is assumed to be infinite.

As shown in Figs. 1 and 2, z is the heave direction, and is positive upward the still water surface, l is half of the horizontal distance between the two springs, l_0 is the original length of both springs, θ is the inclination of the spring with respect to the origin, and k_0 is the stiffness of the spring. And the stiffness of linear PTO system is chosen as $K=2k_0$. For both linear and nonlinear PTO systems, the damper is linear along the direction of the heaving oscillation.

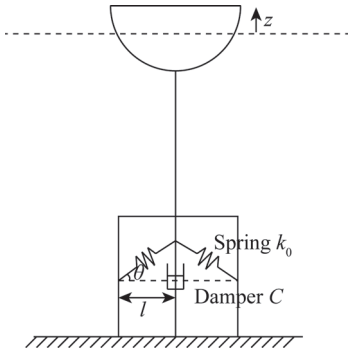

Fig. 1. Wave energy converter with nonlinear snap-through PTO mechanism.

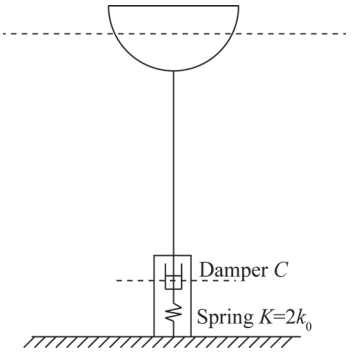

Fig. 2. Wave energy converter with linear PTO mechanism.

3. Static Characteristics of Snap-Through Mechanism

Fig. 3 shows the nonlinear snap-through oblique spring systems with an axial force acting on both springs. Then the total axial force F as a function of z is given by

$$F = 2k_0(\sqrt{z^2 + l^2} - l_0)\sin\theta, \tag{1}$$

where,

$$\sin\theta = \frac{z}{\sqrt{z^2 + l^2}}. \tag{2}$$

Substituting Eq. (2) into Eq. (1),

$$F = 2k_0\left(1 - \frac{l_0}{\sqrt{z^2 + l^2}}\right)z\ . \tag{3}$$

And Eq. (3) can be expressed in the dimensionless form as:

$$F^* = \left(1 - \frac{1}{\sqrt{z^{*2} + \gamma^2}}\right) z^*, \tag{4}$$

where, $F^*=F/(2k_0l_0)$, $z^*=z/l_0$, and $\gamma = l/l_0$. Fig. 4 shows the non-dimensional axial force F^* as the function of dimensionless displacement z^*. $\gamma = 0$ corresponds to the linear spring with the stiffness being always positive since the force acts along the axis of the deformation of the spring. When $0<\gamma<1$, a region exists where the composition of forces due to deformation of springs is in the same direction as the motion, as the springs are displaced from z=0. Thus, it leads to a negative stiffness. And as $\gamma \geq 1$, the stiffness of the system is always positive. The dimensionless stiffness of the system can be obtained by

$$K^* = \frac{\mathrm{d}F^*}{\mathrm{d}z^*} = 1 - \frac{\gamma^2}{(z^{*2} + \gamma^2)^{3/2}}, \tag{5}$$

where $K^*=K/(2k_0)$ and $K=\mathrm{d}F/\mathrm{d}z$ is the physical stiffness of the system shown in Fig. 3.

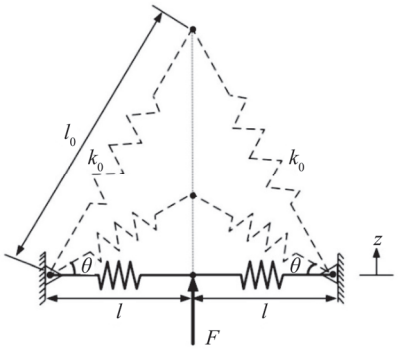

Fig. 3. Arrangement of two oblique springs for the snap-through mechanism.

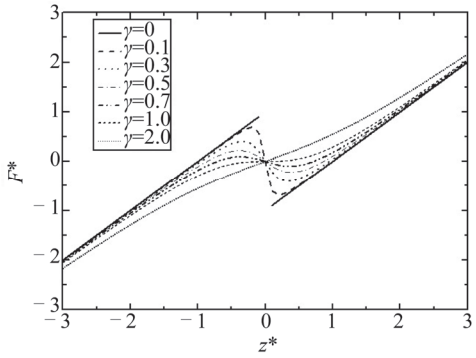

Fig. 4. Dimensionless total axial force F^* versus non-dimensional displacement z^*.

The non-dimensional nonlinear stiffness of the snap-through oblique spring system for various γ is shown in Fig. 5. The strength of the negative stiffness depends on the value of γ. As shown in Fig. 5, the smaller the value of γ is, the more negative the stiffness K^* will be. When $\gamma \geq 1$, the region for negative stiffness disappears. Let K^*=0, and then the critical displacement z_c^* at which the snap-through occurs is obtained as follows:

$$z_c^* = \gamma^{2/3}\sqrt{1-\gamma^{2/3}}. \tag{6}$$

Although the strength of the negative stiffness becomes larger as $\gamma\,(0<\gamma<1)$ becomes smaller, the range of the negative stiffness nevertheless becomes smaller.

For the nonlinear oblique spring system shown in Fig. 3, the potential energy can be expressed as:

$$E_\mathrm{p} = 2\left[\frac{1}{2}k_0(\sqrt{z^2+l^2} - l_0)^2\right]. \tag{7}$$

The non-dimensional form of the potential energy $E_\mathrm{p}^* = E_\mathrm{p}\big/\left(k_0 l_0^{\,2}\right)$ is as follows:

$$E_\mathrm{p}^* = (\sqrt{z^{*2}+\gamma^2} - 1)^2. \tag{8}$$

Let $\mathrm{d}E_{\mathrm{p}}^{*}/\mathrm{d}z^{*}=0$, and three values of z^{*} are given by

$$z_1^{*}=-\sqrt{1-\gamma^2}\ ,\quad z_2^{*}=0\ ,\quad z_3^{*}=\sqrt{1-\gamma^2}\ . \tag{9}$$

The non-dimensional potential energy E_{p}^{*} versus z^{*} for $\gamma=0.1$ and $\gamma=0.7$ is shown in Fig. 6. The snap-through oblique spring system is characteristic of double-well potential. For three equilibrium positions, z_1^{*} and z_3^{*} are stable, while z_2^{*} is unstable. As a result, there may be two possible types of motions for the system. One is local motion near one of the two stable equilibrium positions, the other is the global motion oscillating from one stable equilibrium position to another via the unstable one. The local oscillation may occur when the input is so small that the system cannot pass the potential barrier. In general, the local oscillation will be periodic under a periodic excitation. The global oscillation is induced when the input is large enough for the system to pass the potential barrier from one stable equilibrium position to another. Unlike local motion, the global oscillation may be either periodic or chaotic even if the input is periodic.

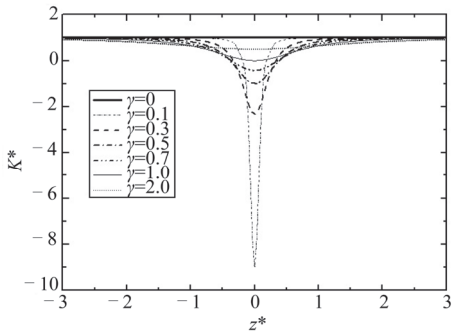

Fig. 5. Dimensionless stiffness of the system K^{*} versus non-dimensional displacement z^{*}.

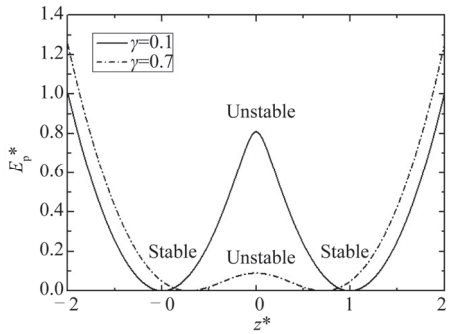

Fig. 6. Non-dimensional potential energy E_{p}^{*} versus dimensionless displacement z^{*}.

4. Dynamic Responses of Linear and Nonlinear Converters in Regular Waves

4.1 Governing Equations

As stated before, for the nonlinear wave energy converter shown in Fig. 1, only the heave oscillation is considered for simplified cases. For a nonlinear dynamic system in regular waves, the frequency domain analysis is not applicable. Thus, time domain model, which was first introduced by Cummins (1962) to ship motions in wavy seas, is used to analyze the dynamic response of the oscillating wave energy converters with nonlinear snap-through PTO systems in regular waves. The heave motion of the hemispherical wave energy converter with nonlinear snap-through PTO system can be expressed as:

$$\left[m+A_z(\infty)\right]\ddot{z}(t)+\int_0^t k_z(t-\tau)\dot{z}(\tau)\mathrm{d}\tau+C\dot{z}(t)+\rho gSz(t)+K\left(1-\frac{l_0}{\sqrt{l^2+z^2}}\right)z=f_{\mathrm{dzregular}}\,. \tag{10}$$

And the governing equation of heave oscillation for linear wave energy converter is

$$\left[m+A_z(\infty)\right]\ddot{z}(t)+\int_0^t k_z(t-\tau)\dot{z}(\tau)\mathrm{d}\tau+C\dot{z}(t)+(\rho gS+K)z(t)=f_{\mathrm{dzregular}}\,, \tag{11}$$

where, t is time. z, $\dot{z}$ and $\ddot{z}$ are the displacement, velocity and acceleration for the heave oscillation, respectively; $A_z(\infty)$ are the limiting value of the added mass $A_z(\omega)$ for the circular frequency of the incident wave $\omega=\infty$; $f_{\mathrm{dz\ regular}}$ is the wave excitation force of the hemispherical converter consisting of Froude–Kriloff forces and diffraction forces due to the incident regular waves; C is the damping coefficient for both the nonlinear and linear PTO systems; K is the stiffness of spring for the linear PTO system, while twice the stiffness of each spring for the nonlinear PTO mechanism. This is convenient for the comparison of linear and nonlinear PTO system; ρ is the density of water; g is the acceleration of gravity; m is the mass of the hemispherical floater with values of $2\rho\pi R^3/3$, R being the radius of the hemisphere; S is the area of the cross section of the hemisphere and $S=\pi R^2$; and $k_z(t)$ is the retardation function indicating the memory effect of fluid in the radiation forces, which can be written as:

$$k_z(t)=\frac{2}{\pi}\int_0^{\infty}B_z(\omega)\cos(\omega t)\mathrm{d}\omega\ , \tag{12}$$

where, $B_z(\omega)$ is the radiation damping of the hemispherical floater oscillating in the heave direction.

In the following calculation, the water depth is assumed to be infinite. For both linear and nonlinear converters, the radius of the hemisphere is R=5 m; the density of water is ρ=1025 kg/m^3; the gravity acceleration is g=9.81 m/s^2; the mass of the hemispherical converter is the same as the mass of displaced water in calm surface, $m=2\rho\pi R^3/3$; and the area of the cross section of the hemisphere is $S=\pi R^2$. As indicated by Vicente *et al.* (2013), the equivalent stiffness of the PTO system is usually around ten percent of the hydrostatic coefficient of the floater. Thus, in our calculation, $K=0.1\rho gS$.

For given regular waves of angular frequency ω and amplitude A_ω, the moduli of wave excitation force is proportional to the amplitude of the incident waves. This may be written as $\left|f_{\mathrm{dz\ regular}}\right|=\Gamma_z(\omega)A_\omega$, where $\left|f_{\mathrm{dz\ regular}}\right|$ is the moduli of the wave excitation force, and $\Gamma_z(\omega)$ is the excitation force coefficient. Hulme (1982) gave the tabulated values, as well as asymptotic expressions, for the coefficients of the added mass and radiation damping of a floating hemisphere oscillating in deep water in dimensionless form. And in our calculations in this paper, these values given by Hulme (1982) are adopted. Falnes (2002) studied the excitation force coefficients of the heave oscillation for an axisymmetric body in deep water and related the excitation force coefficients with radiation damping, known as Haskind's relation,

$$\Gamma_z(\omega)=\left[\frac{2g^3\rho B_z(\omega)}{\omega^3}\right]^{1/2}. \tag{13}$$

The added mass and radiation damping coefficients, as well as the wave excitation force for the hemisphere oscillating in heave direction are shown in Fig. 7.

It can be seen from Fig. 7 that for a hemispherical floater oscillating in the heave direction, the added mass decreases as the circular frequency of incident waves increases, reaching its lowest point at the circular frequency equal to 1.8 rad/s. Then the added mass of the floater increases with the increase of frequency. For the radiation damping, the maximum value occurs when the frequency of the incident waves equals 1.4 rad/s. And the wave excitation force experiences a downward trend, approximating to

zero as the circular frequency of incident waves approaches to infinite.

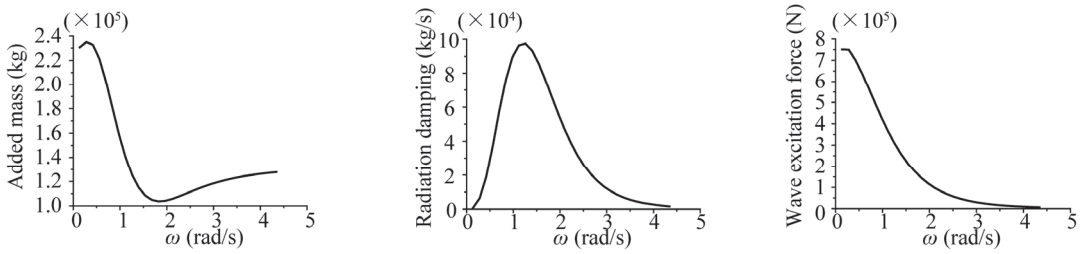

Fig. 7. Hydrodynamic quantities for the hemispherical floater oscillating in the heave direction (Hulme (1982) and Falnes (2002)).

For the oscillation of linear wave energy converter shown in Eq. (11), it can be expressed in the frequency domain as follows:

$$\left[m + A_z(\omega)\right]\ddot{z} + B_z(\omega)\dot{z} + \rho g S z = f_{\mathrm{dz\ regular}} - C\dot{z} - Kz\,. \tag{14}$$

Suppose Z and $F_{\mathrm{dz\ regular}}$ is the complex amplitude of z and $f_{\mathrm{dz\ regular}}$. Then by solving Eq. (14), we can obtain

$$Z = \frac{F_{\mathrm{dz\ regular}}}{-\omega^2\left[m + A_z(\omega)\right] + \rho g S + K + \mathrm{i}\omega\left[B_z(\omega) + C\right]}\,. \tag{15}$$

The time-averaged power absorbed by the linear wave energy converter is given by Evans (1980) as follows:

$$P = \frac{1}{2}C\omega^2\left|Z\right|^2 = \frac{1}{8B_z(\omega)}\left|F_{\mathrm{dz\ regular}}\right|^2 - \frac{B_z(\omega)}{2}\left|U - \frac{F_{\mathrm{dz\ regular}}}{2B_z(\omega)}\right|^2, \tag{16}$$

where, $U=\mathrm{i}\omega Z$ is the complex amplitude of the heave oscillation velocity of the floater. This shows that, for a given floater and given incident wave, which means that the fixed B_z and $F_{\mathrm{dz\ regular}}$, the time-averaged absorbed power reaches its maximum value as $U=F_{\mathrm{dz\ regular}}/(2B_z)$. Substituting this into Eq. (15), then

$$\omega = \left[\frac{\rho g S + K}{m + A_z(\omega)}\right]^{1/2}; \tag{17}$$

$$C = B_z(\omega)\,. \tag{18}$$

Eq. (17) means a resonance condition for the maximum power absorption. And Eq. (18) shows that the linear damping coefficient of the PTO system should equal the radiation damping of the floater in order to gain the maximum power.

4.2 State Space Model

The convolution terms in the time domain model shown in Eqs. (10) and (11) make it inconvenient for the analysis of the dynamic response of the converters. Thus, the state-space model (Alves, 2012) is used to replace the convolution term. A general state-space model has the form,

$$\begin{cases} \dot{\boldsymbol{X}}(t) = \boldsymbol{A}'\boldsymbol{X}(t) + \boldsymbol{B}'u(t) \\ y(t) = \boldsymbol{C}'\boldsymbol{X}(t) \end{cases} \tag{19}$$

where $u(t)$ and $y(t)$ are called the input and output respectively of the state-space. $\boldsymbol{X}(t)$ is the state

vector. $\boldsymbol{A}'$, $\boldsymbol{B}'$ and $\boldsymbol{C}'$ are the coefficients of the state space. The convolution term in Eqs. (10) and (11) is replaced by the state-space model as:

$$\begin{cases} \dot{\boldsymbol{X}}(t) = \boldsymbol{A}'\boldsymbol{X}(t) + \boldsymbol{B}'\dot{z}(t) \\ I_z(t) = \boldsymbol{C}'\boldsymbol{X}(t) \end{cases} \tag{20}$$

where, $I_z(t) = \int_0^t k_z(t-\tau)\dot{z}(\tau)\mathrm{d}\tau$ is the radiation force considering the memory effects of the fluid in time domain.

The problem now is to solve the matrices $\boldsymbol{A}'$, $\boldsymbol{B}'$ and $\boldsymbol{C}'$ to approximate the convolution model, which is also called system identification (Taghipour *et al*., 2008). In the frequency domain, the kernel has the relationship with the coefficients of the added mass and damping, expressed as follows:

$$k_z(\mathrm{j}\omega) = \int_0^\infty k_z(\tau)\mathrm{e}^{-\mathrm{j}\omega\tau}\mathrm{d}\tau = B_z(\omega) + \mathrm{j}\omega\left[A_z(\omega) - A_z(\infty)\right], \tag{21}$$

where, $k_z(\mathrm{j}\omega)$ is the frequency response of the convolutions using Fourier transform. j is the imaginary part. The least square technique is then used to find a rational function $\hat{k}_z$ that approximates $k_z(\mathrm{j}\omega)$ for the given set of circular frequencies following the restrictions given by Perez and Fossen (2011). This approximation is restricted to imaginary values, and the rational function is defined, using $s = \mathrm{j}\omega$, as:

$$\hat{k}_z(s,\boldsymbol{\theta}) = \frac{p_{n-1}s^{n-1} + p_{n-2}s^{n-2} + \cdots + p_1 s}{s^n + q_{n-1}s^{n-1} + \cdots + q_0}, \tag{22}$$

where, n is the order of the system. Eq. (22) is also called the transfer function. As long as the coefficients $\boldsymbol{\theta} = [p_{n-1}, p_{n-2}, \cdots, p_1, q_{n-1}, q_{n-2}, \cdots, q_0]$ are found using the least square method, the matrix and vectors of state space model which approximate the convolution integral can be written as:

$$\boldsymbol{A}' = \begin{bmatrix} -q_{n-1} & -q_{n-2} & -q_{n-3} & \cdots & -q_1 & -q_0 \\ 1 & 0 & 0 & \cdots & 0 & 0 \\ 0 & 1 & 0 & \cdots & 0 & 0 \\ \vdots & \vdots & \vdots & \cdots & 0 & 0 \\ 0 & 0 & 0 & \cdots & 1 & 0 \end{bmatrix}; \quad \boldsymbol{B}' = \begin{bmatrix} 1 \\ 0 \\ 0 \\ \vdots \\ 0 \end{bmatrix}; \quad \boldsymbol{C}' = \left[p_{n-1}, p_{n-2}, \cdots, p_1, 0\right]. \tag{23}$$

For the hemispherical wave energy converter in this study, by the method of iteration, the order of the system is chosen $n = 5$, providing a rather good identification of the retardation function in the frequency domain. The identification results of the order $n = 5$ are shown in Figs. 8 and 9.

As shown in the two figures, the identification results agree well with the original data. The results of coefficients for the state space model in Eq. (20) are

$$\boldsymbol{A}' = \begin{bmatrix} -3.8400 & -7.1237 & -5.8309 & -1.9262 & -0.0538 \\ 1 & 0 & 0 & 0 & 0 \\ 0 & 1 & 0 & 0 & 0 \\ 0 & 0 & 1 & 0 & 0 \\ 0 & 0 & 0 & 1 & 0 \end{bmatrix}; \quad \boldsymbol{B}' = \begin{bmatrix} 1 \\ 0 \\ 0 \\ \vdots \\ 0 \end{bmatrix};$$

$$\boldsymbol{C}' = \begin{bmatrix} 92160 & 426370 & 176590 & 4070 & 0 \end{bmatrix}. \tag{24}$$

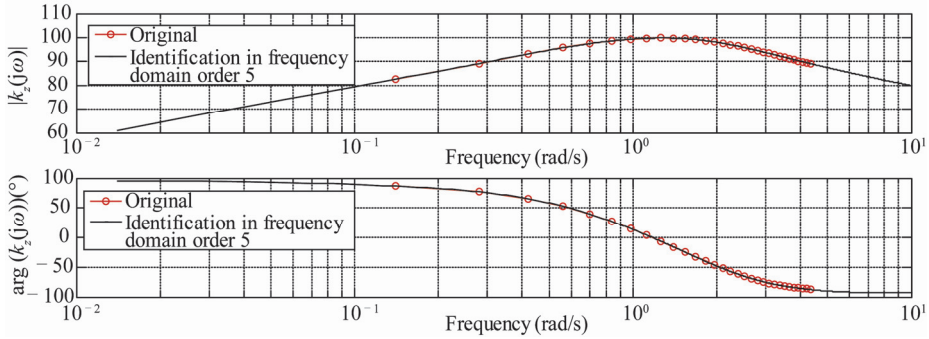

Fig. 8. Identification of the retardation function in the frequency domain: the upper one is the amplitude of $k_z(j\omega)$; the lower one is the angle of $k_z(j\omega)$.

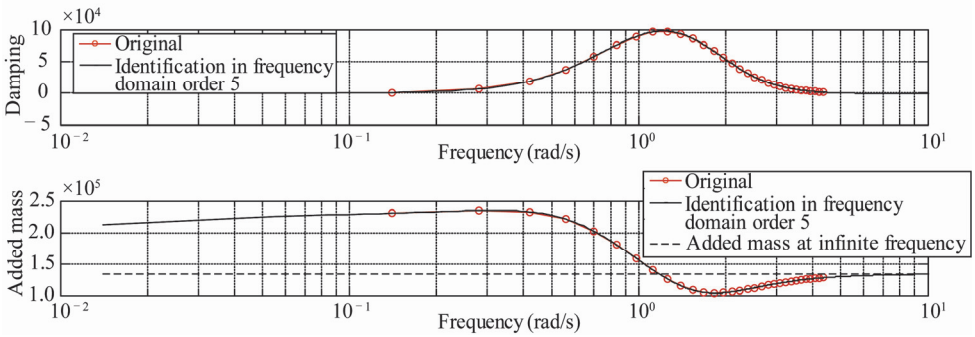

Fig. 9. Identification results of the added mass and radiation damping in the frequency domain: the upper one is the radiation damping; the lower one is the added mass.

As a result, Eq. (10) and Eq.(11) can be replaced by

$$\left[m+A_z(\infty)\right]\ddot{z}(t)+\boldsymbol{C'X}(t)+C\dot{z}(t)+\rho gSz(t)+K\left(1-\frac{l_0}{\sqrt{l^2+z^2}}\right)z=f_{\mathrm{d}z\ \mathrm{regular}};$$

$$\dot{\boldsymbol{X}}(t)=\boldsymbol{A'X}(t)+\boldsymbol{B'}\dot{z}(t); \tag{25}$$

$$\left[m+A_z(\infty)\right]\ddot{z}(t)+\boldsymbol{C'X}(t)+C\dot{z}(t)+(\rho gS+K)z(t)=f_{\mathrm{d}z\ \mathrm{regular}};$$

$$\dot{\boldsymbol{X}}(t)=\boldsymbol{A'X}(t)+\boldsymbol{B'}\dot{z}(t). \tag{26}$$

Denote a vector $\boldsymbol{\lambda}$ with the dimension of 7×1, and $\boldsymbol{\lambda}=[z\ \dot{z}\ \boldsymbol{X}^{\mathrm{T}}]^{\mathrm{T}}$. Then Eq. (25) is re-expressed as:

$$\dot{\boldsymbol{\lambda}}=\boldsymbol{f}(\boldsymbol{\lambda})+\boldsymbol{Q} \tag{27}$$

with $f_1(\boldsymbol{\lambda})=\lambda_2$;

$$f_2(\boldsymbol{\lambda})=-\frac{\rho gS}{m+A_z(\infty)}\lambda_1-\frac{K}{m+A_z(\infty)}\left(1-\frac{l_0}{\sqrt{l^2+\lambda_1^2}}\right)\lambda_1-\frac{C}{m+A_z(\infty)}\lambda_2-\frac{\boldsymbol{C'}}{m+A_z(\infty)}\boldsymbol{X};$$

$$\left[f_3\ \ f_4\ \ f_5\ \ f_6\ \ f_7\right]^{\mathrm{T}}=\boldsymbol{A'X}+\boldsymbol{B'}\lambda_2 \text{ and } \boldsymbol{Q}=\left[0\quad \frac{f_{\mathrm{d}z\ \mathrm{regular}}}{m+A_z(\infty)}\quad \boldsymbol{0}\right]^{\mathrm{T}}.$$

Eq. (26) is re-expressed as:

$$\dot{\boldsymbol{\lambda}} = \boldsymbol{\Phi}\boldsymbol{\lambda} + \boldsymbol{Q} \tag{28}$$

with $\boldsymbol{\Phi} = \begin{bmatrix} 0 & 1 & 0 \\ -\dfrac{\rho g S + K}{m + A_z(\infty)} & -\dfrac{C}{m + A_z(\infty)} & -\dfrac{\boldsymbol{C'}}{m + A_z(\infty)} \\ 0 & \boldsymbol{B'} & \boldsymbol{A'} \end{bmatrix}$.

The displacement and velocity of the linear and nonlinear systems can be numerically achieved for discrete time by solving Eqs. (27) and (28) using the fourth-order Runge–Kutta method. And the initial conditions are assumed that $z = 0$ and $\dot{z} = 0$. The averaged power harvested by the device for both linear and nonlinear snap-through mechanisms is obtained numerically using the expression for power dissipated by the damper as follows:

$$P = \frac{1}{T}\int_0^T C\dot{z}^2 \mathrm{d}t \,. \tag{29}$$

4.3 Analysis of Results

The original length of both springs shown in Fig. 1 is l_0=10 m. Finally the nonlinear parameter γ is chosen a set of values in the interval (0, 1) in order to study its effects on the power capture by wave energy converter with nonlinear snap-through PTO mechanisms.

For the resonance condition of the linear system as indicated by Eqs. (17) and (18), the resonance angular frequency ω_0=1.516 rad/s. Three wave amplitudes of 0.5 m, 1 m, and 3 m are chosen to study the effects of the wave amplitude on the power capture of the oscillating wave energy converter with nonlinear snap-through PTO mechanism. And according to Eqs. (17) and (18), the optimum damping coefficient of the linear PTO system is C_{opt}=87480 rad/s. The influence of 25% variation of the damping coefficient C_{opt} is considered.

The averaged power obtained by the hemispherical converter with both linear and nonlinear PTO systems, as well as the ratio of the linear and nonlinear converters are shown in Figs. 10–15.

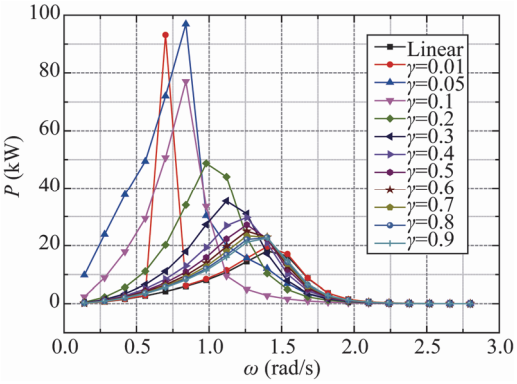

Fig. 10. Power captured by both linear and nonlinear wave energy converters for different circular frequencies and nonlinear parameter γ with the wave amplitude 0.5 m and C = 87480 kg/s.

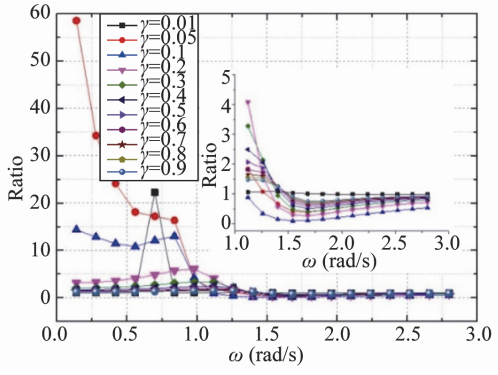

Fig. 11. Ratio of power captured by nonlinear wave energy converters with linear converters for different circular frequencies and nonlinear parameter γ with the wave amplitude 0.5 m and C = 87480 kg/s.

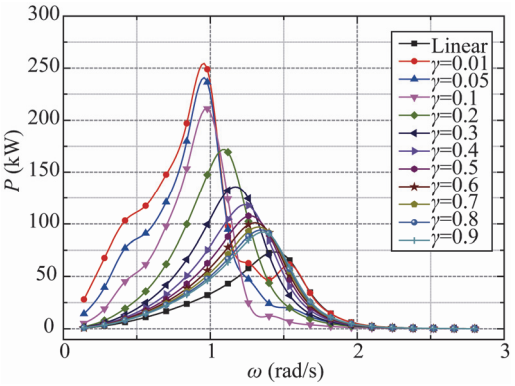

Fig. 12. Power captured by both linear and nonlinear wave energy converters for different circular frequencies and nonlinear parameter γ with the wave amplitude 1 m and C = 87480 kg/s.

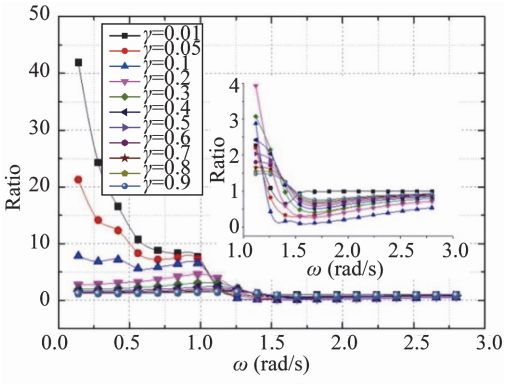

Fig. 13. Ratio of power captured by nonlinear wave energy converters with linear converters for different circular frequencies and nonlinear parameter γ with the wave amplitude 1 m and C = 87480 kg/s.

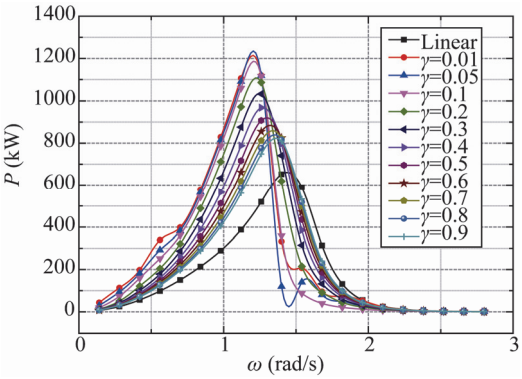

Fig. 14. Power captured by both linear and nonlinear wave energy converters for different circular frequencies and nonlinear parameter γ with the wave amplitude 3 m and C = 87480 kg/s.

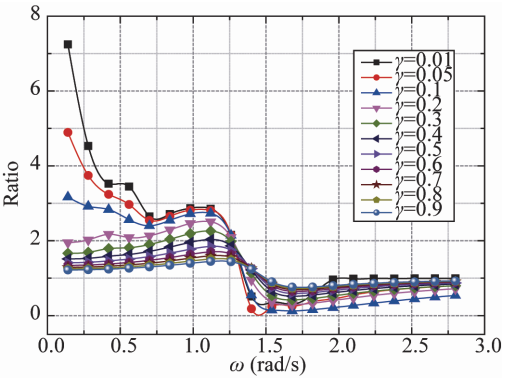

Fig. 15. Ratio of power captured by nonlinear wave energy converters with linear converters for different circular frequencies and nonlinear parameter γ with the wave amplitude 3 m and C = 87480 kg/s.

Figs. 10–15 illustrate the averaged power obtained by the oscillating wave energy converters with both linear and nonlinear snap-through PTO mechanism, as well as the ratio of power captured by the two wave energy converters. And the wave amplitude varies from 0.5 m to 3 m. The equivalent damping coefficient of PTO systems is chosen as the optimum values of the linear converters, 87480 kg/s.

The nonlinear parameter γ has great effects on the power capture of the oscillating wave energy converters with the nonlinear snap-through PTO mechanism. For a given wave amplitude and damping coefficient of PTO systems, the smaller the value of γ (larger than 0 and smaller than 1) is, the larger is the amount of the power captured by nonlinear converters for the frequency of incident waves lower than the resonance one. Whereas the effect of γ can be neglected on the power capture at high incident frequency region. Unlike the linear PTO system, the maximum power of which is obtained at the natural frequency of the converter being 1.4 rad/s, the nonlinear oscillating wave energy converter gains its maximum power at a given frequency smaller than 1.4 rad/s. And as the value of γ becomes larger, the

optimum frequency approaches to the natural frequency of the linear systems.

By comparing Figs. 10–11, Figs. 12–13 and Figs. 14–15, it can be found that the wave amplitude also influences the power capture by nonlinear and linear converters. Since the value of the nonlinear parameter γ is smaller than 0.1 (0.01 and 0.05), the ratio of the power between nonlinear and linear converters is larger than 5 at low incident frequency region for the wave amplitude being 1 m. However, the value is smaller than 4 when the wave amplitude is 3 m. For the nonlinear parameter γ approaching to 1, the effect of the wave amplitude on the ratio can be neglected. The optimum frequency at which the maximum power is captured by the nonlinear converters is also affected by the wave amplitude. As the wave amplitude increases from 0.5 m to 3 m, the value of the optimum frequency is more and more approaching the resonance one.

Fig. 16 shows the power captured by both linear and nonlinear wave energy converters for three different damping coefficients of PTO systems. It can be seen from Fig. 16 that, for the oscillating wave energy converter with both linear and nonlinear snap-through PTO systems, appropriate enlarging the value of damping coefficient of PTO system near the optimum value leads to an increase in the power capture at both low and high incident frequency region. Whereas the value of the averaged power obtained becomes smaller as the damping coefficient decreases.

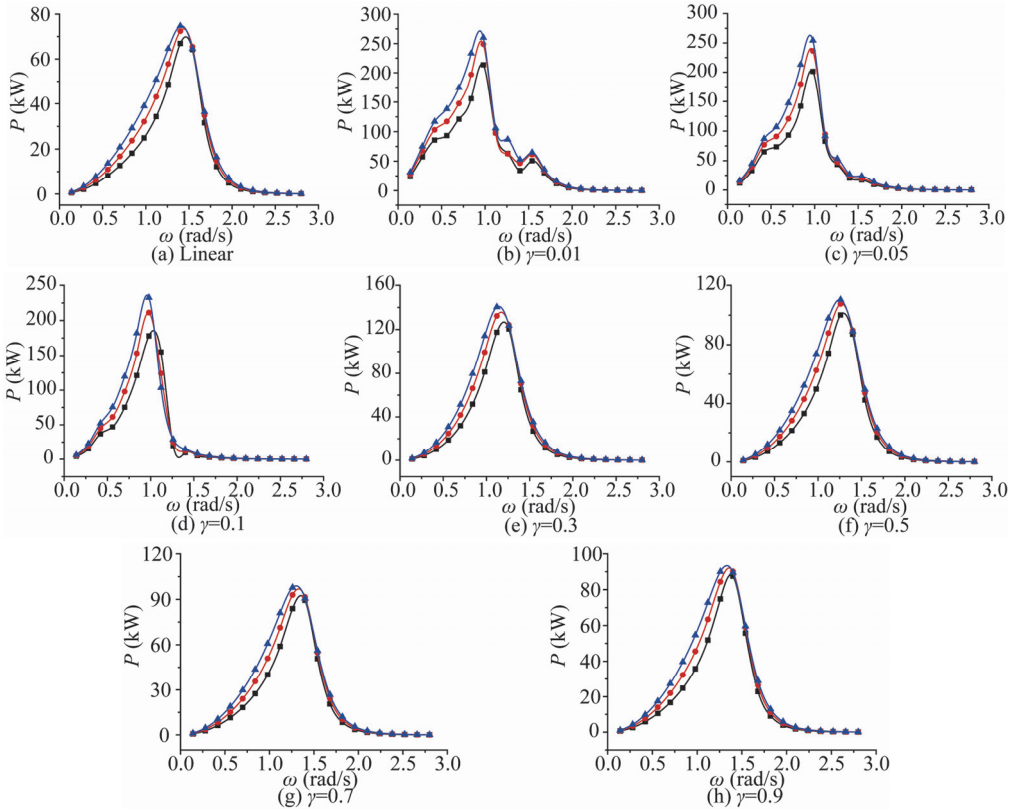

Fig. 16. The averaged power captured by both linear and nonlinear wave energy converters for three different values of damping coefficient of PTO systems (black line: C = 65880 kg/s; red line: C = 87480 kg/s; blue line: C = 109800 kg/s).

Figs. 17–19 are some illustrated examples of the steady time history of the heaving displacement and velocity, as well as the phase portrait for linear and nonlinear wave energy converters with C=87480 kg/s and A_ω=1 m at three different incident frequencies. For Figs. 18 and 19, the motion response of the nonlinear converter has returned to the sinusoidal characteristics which are similar to that of the linear converter after $\gamma \geq 0.3$, thus, the motion response of $\gamma = 0.4$ and $\gamma = 0.6$ are omitted.

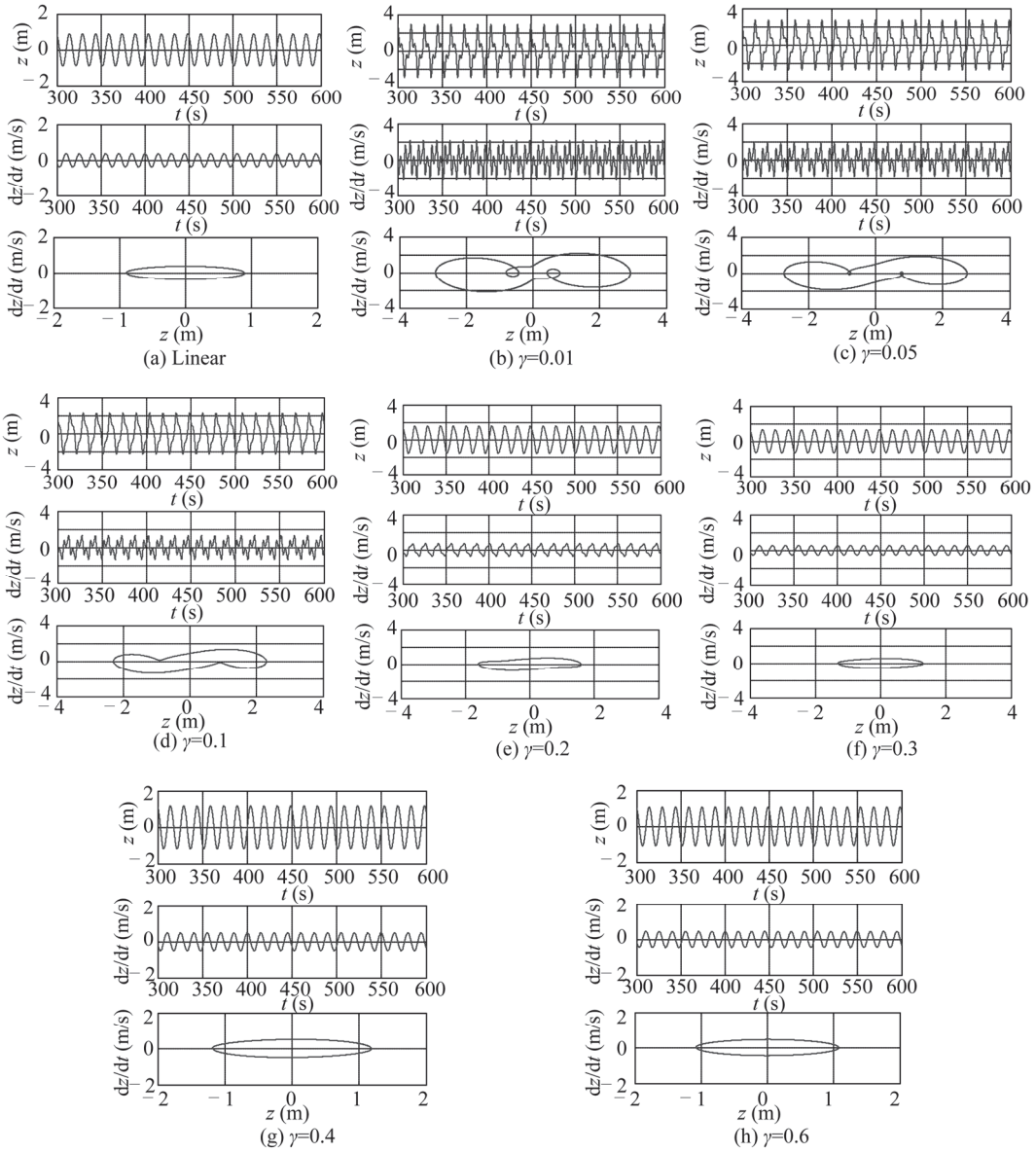

Fig. 17. Steady time history of the heaving displacement and velocity, as well as the phase portrait for linear and nonlinear wave energy converters with C=87480 kg/s, A_ω=1 m and ω=0.42 rad/s.

For the oscillating wave energy converters with the linear PTO systems, the responses of the

displacement and velocity are both sinusoidal with the same frequency as that of incident regular waves, and thereby the phase portrait is characteristic of elliptical trajectory. While for the wave energy converter with nonlinear snap-through PTO systems, the responses are no longer sinusoidal for certain values of the nonlinear parameter γ. And the trajectory of the phase portrait is not elliptical. At low incident frequency (ω=0.42 rad/s), the time history of the displacement and velocity is somewhat chaotic with several values of the nonlinear parameter γ. As the value of the nonlinear parameter γ becomes larger, the chaotic strength of the response is weakened, which is verified by the fact that the phase portrait approaches to an elliptical trajectory. And the responses return to be sinusoidal as γ is larger than 0.4. At the resonance frequency (ω=1.4 rad/s), the case is similar. However, the response becomes sinusoidal again as long as γ is larger than 0.1. Finally at high frequency (ω=2.24 rad/s), the oscillation of the nonlinear wave energy converter is local, the equilibrium position of which is around 0.8 m, for γ being smaller than 0.1. This may be due to the fact that the potential barrier shown in Fig. 6 is too high for the converter to pass through, leading to a local oscillation around one of stable equilibrium positions. For the high incident frequency, all the time histories of the displacement and velocity are sinusoidal, which are different from those at low and resonance frequency.

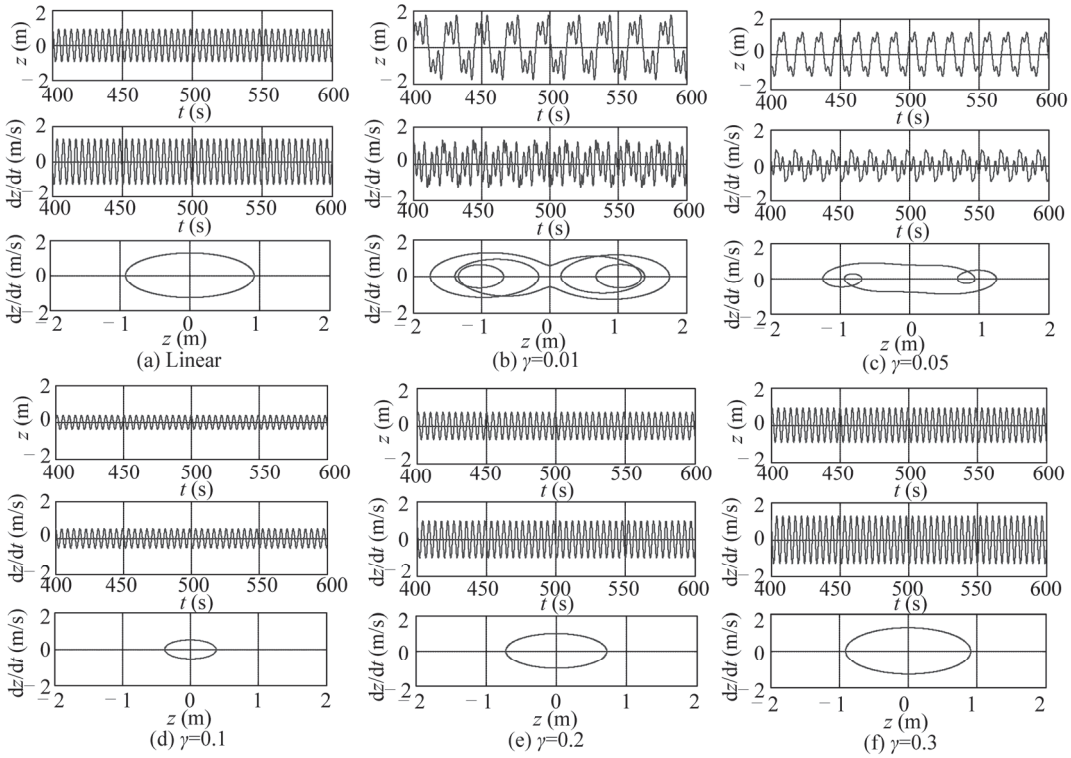

Fig. 18. Steady time history of the heaving displacement and velocity, as well as the phase portrait for linear and nonlinear wave energy converters with C = 87480 kg/s, A_ω=1 m and ω=1.4 rad/s.

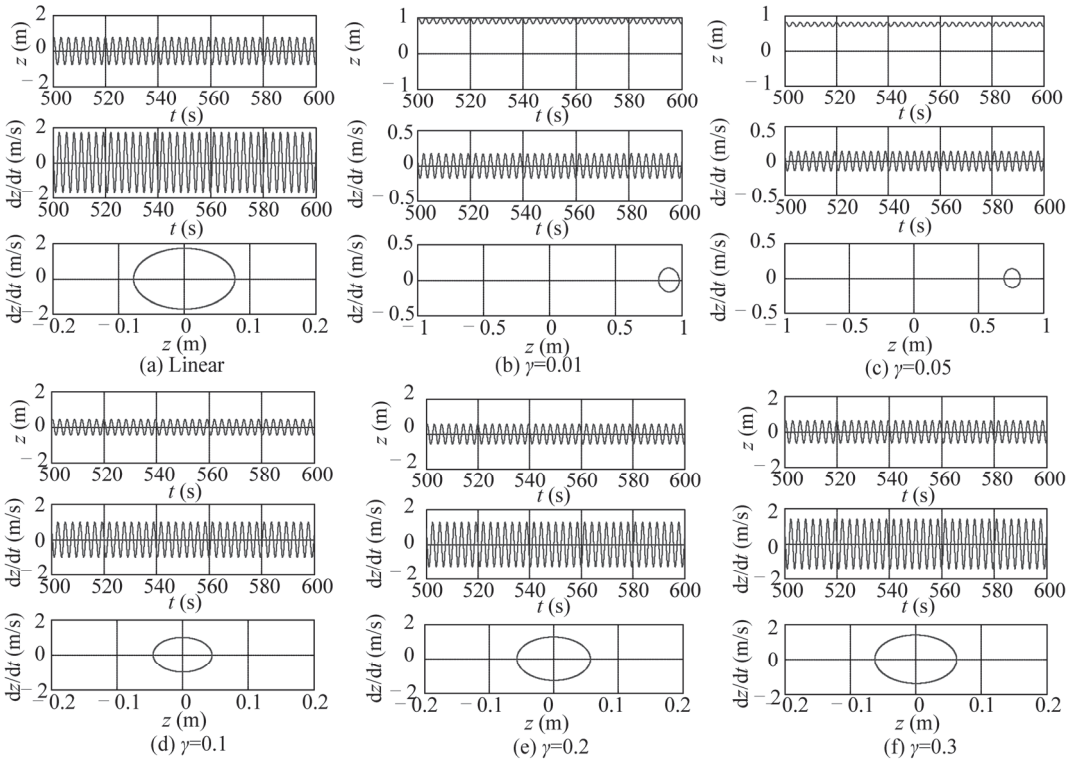

Fig. 19. Steady time history of the heaving displacement and velocity, as well as the phase portrait for linear and nonlinear wave energy converters with C=87480 kg/s, A_ω=1 m and ω=2.24 rad/s.

5. Conclusions

A nonlinear snap-through mechanism consisting of two symmetrically oblique springs and a linear damper was applied in the PTO system of the oscillating-body wave energy converters. The snap-through mechanism can generate the negative stiffness, which is of benefit to the energy harvesting. And the nonlinear parameter γ affects the strength of the negative stiffness, as well as the oscillation range in which the stiffness is negative. A small value of γ generates a strong strength but a small range of the negative stiffness. Unlike the linear PTO system, the nonlinear snap-through system is characteristic of double well potential with two stable and one unstable equilibrium positions.

The averaged energy harvested by the oscillating wave energy converter with nonlinear snap-through PTO systems is much more than that by linear ones if the frequency of regular waves is smaller than the resonance frequency. As the frequency of incident regular waves exceeds the resonance one, the power captured by nonlinear converters is slightly smaller than that by linear converters. The nonlinear parameter γ has great effects on the power capture of the oscillating wave energy converters with the nonlinear snap-through PTO mechanism. Smaller value of γ generates larger amount of the power captured by nonlinear converters for the frequency of incident waves lower than the resonance one. And

this influence can be neglected on the power capture at high incident frequency region. The ratio of power between nonlinear and linear converters becomes relatively smaller as the wave amplitude increases.

For the wave energy converter with nonlinear snap-through PTO systems, the responses are periodically inter well for certain values of the nonlinear parameter γ at low and resonance frequency region. At high frequency region, the oscillation becomes local at one of the stable equilibrium positions for γ being smaller than 0.1, although the responses are sinusoidal for all values of γ.

References

Alves, M., 2012. *Numerical Simulation of the Dynamics of Point Absorber Wave Energy Converters Using Frequency and Time Domain Approaches*, Ph. D. Thesis, Universidade Tecnica de Lisboa.

Burrow, S. G. and Clare, L. R., 2007. A resonant generator with nonlinear compliance for energy harvesting in high vibrational environments, *IEEE International Conference on Electric Machines & Drive Conference*, Antalya, Turkey, 715–720.

Cummins, W. E., 1962. The impulse response function and ship motions, *Schiffstechnik*, **9**, 101–109.

Evans, D. V., 1980. Some analytic results for two and three dimensional wave energy absorbers, in: Count, B. (Ed.), *Power from Sea Waves*, Academic Press, London, 213–249.

Falcão, A. F. O., 2010. Wave energy utilization: a review of the technologies, *Renewable and Sustainable Energy Reviews*, **14**(3): 899–918.

Falnes, J., 2002. *Ocean Waves and Oscillating Systems*, Cambridge University Press, Cambridge.

Gomes, R. P. F., Henriques, J. C. C., Gato, L. M. C. and Falcão, A. F. O., 2012. Hydrodynamic optimization of an axisymmetric floating oscillating water column for wave energy conversion, *Renewable Energy*, **44**, 328–339.

Harne, R. L. and Wang, K. W., 2013. A review of the recent research on vibration energy harvesting via bistable systems, *Smart Materials and Structures*, **22**(2): 023001.

Hulme, A., 1982. The wave forces acting on a floating hemisphere undergoing forced periodic oscillations, *J. Fluid Mech.*, **121**, 443–463.

Ma, T. W., 2011. Opportunities for using nonlinear oscillators to enhance energy harvesting from impulsively loaded structures, *Journal of Systems and Control Engineering*, **225**(4): 467–474.

Mann, B. P. and Sims, N. D., 2009. Energy harvesting from the nonlinear oscillation of magnetic levitation, *Journal of Sound and Vibration*, **319**(1–2): 515–530.

Perez, T., and Fossen, T. I., 2011. Practical aspects of frequency-domain identification of dynamic models of marine structures from hydrodynamic data, *Ocean Eng.*, **38**(2): 426–435.

Ramlan, R., Brennan, M. J., Mace, B. R. and Kovacic, R., 2010. Potential benefits of a nonlinear stiffness in an energy harvesting device, *Nonlinear Dynamics*, **59**(4): 545–558.

Taghipour, R., Perez, T. and Moan, T., 2008. Hybrid frequency–time domain models for dynamic response analysis of marine structures, *Ocean Eng.*, **35**(7): 685–705.

Vicente, P. C., Falcão, A. F. O. and Justino, P. A. P., 2013. Nonlinear dynamics of a tightly moored point-absorber wave energy converter, *Ocean Eng.*, **59**, 20–36.

Zhang, D. H., Li, W., Zhao, H. T., Bao, J. W. and Lin, Y. G., 2014. Design of a hydraulic power take-off system for the wave energy device with an inverse pendulum, *China Ocean Eng.*, **28**(2): 283–292.

Zhang, Y. Q., Sheng, S. W., You, Y. G., Wu, B. J. and Liu, Y., 2014. Research on energy conversion system of floating wave energy converter, *China Ocean Eng.*, **28**(1): 105–113.